Compression of a polymer chain by a small obstacle: The effect of fluctuations on the escape transition

J. Ennis, E. M. Sevick, and D. R. M. Williams
Research School of Chemistry and Research School of Physical Sciences and Engineering, Australian National University, Canberra, ACT 0200, Australia
(Received 21 April 1999)

We describe the escape transition of an ideal chain compressed between finite-sized obstacles. Three different theoretical methods are used and each provides a similar description of the escape transition, as predicted by earlier and less detailed mean-field theories. The first two methods show that thermal fluctuations near the transition can blur what was previously described as a sharp transition. The last method is an exact calculation of the partition function that shows unambiguously the character of the escape transition. This exact calculation overcomes the inherent uncertainties associated with previous theory and computer simulation.
[S1063-651X(99)04911-9]

PACS number(s): 36.20.Ey, 61.25.Hq, 46.32.+x

I. INTRODUCTION

One of the most vigorous research areas in modern soft condensed matter physics over the past decade has been the imaging and manipulation of individual polymer chains [1–3]. This has been made possible by advances in microscopy, particularly in fluorescence microscopy, atomic force microscopy, and optical-magnetic tweezers, and has led to a number of investigations of single macromolecules, particularly those of biological origin, such as DNA and actin. These kind of experiments have inspired new topics for theoretical and computational study. One recent topic is the compression of a surface-tethered polymer chain by an obstacle that is not much larger than the unperturbed chain. This can occur by compressing a chain that is end-tethered to a surface with an atomic force microscope (AFM) tip, or by the impaction of a membrane-tethered biopolymer by a cellular object.

The deformation of a polymer that is compressed between two infinite planar plates is well understood: the chain deforms uniformly within the narrowing slit and the force that the chain imposes on the compressing plates grows monotonically [4,5]. However, the compression of an end-tethered chain by a finite-sized obstacle is very different: the chain deforms nonuniformly and there can be a jump in the compression force [6–15]. When compressed weakly by a finite-sized obstacle, the chain remains fully confined or ''imprisoned'' under the obstacle. However, at intermediate compressions, when the compression energy is high, the chain can reduce its overall energy by forming a stretched umbilical tether from the grafting point to the edge of the disk so that the remaining monomers in the chain have ''escaped'' from underneath the compressing obstacle [6–15]. A jump in the force exerted by the chain upon the obstacle is one signature of the transition from an imprisoned chain to a partially escaped one. There can be a significant energetic barrier to escape depending upon the radius of the obstacle relative to the size of the chain. This barrier arises from the extra energy needed to stretch the chain to the edge of the disk so that at least one monomer can escape. When this barrier is large, i.e., when the disk size is significantly larger than the chain size, but not larger than the fully extended length of the chain, then the problem can be cast as a first-order transition between two ''states'' of the chain: imprisoned and escaped.

A recent series of theory and computer simulation papers have described this escape transition, the chain energy and the compressive force of end-tethered chains under finite obstacles. The initial papers were theoretical and considered chains in good solvent which were compressed by flat-ended circular cylinders and round-ended cylinders [7–9]. Later the theory was extended to tilted, flat-ended obstacles and ideal chains [6]. Implicit to these early theory papers was the assumption of single state occupancy, i.e., at any given compression, the chain was assumed to reside exclusively in the escaped or in the imprisoned state. This simplifying assumption is not valid whenever the difference in energies between the two states is small, particularly near the escape transition. Several simulation studies have more recently appeared [10–14]. While most of these studies confirm the existence of chain escape from underneath the obstacle, the simulations do not recover the sharpness of the transition that was predicted by the mean-field treatment. Indeed, the description of the force profile at or near the escape transition is in question. The mean-field treatments predict a sharp, discontinuous drop in compressive force, while a number of preprints have interpreted computer simulation results in terms of a flat or constant force profile through the transition region.

In this paper we present calculations of the force profile (and other quantities) near the escape transition that refine the coarse-grained mean-field descriptions, are consistent with previous simulations, but differ from some previous interpretations of the data. Because most of the physics of the problem is contained in the ideal chain case, where there are no excluded volume interactions between monomers, and as this is also the simplest case to examine, we focus only upon ideal chains in this paper. Our description is constructed using three different and independent approaches. The first approach, described in the following section, is a simple two-state model which, albeit approximate, provides analytic force profiles which are comparable with recent simulation. The second approach used is described in Sec. III and con-

sists of stochastically generating ''squashed'' chain configurations using computer simulation. And finally, in Sec. IV we numerically evaluate the partition function for finite-sized chains underneath finite-sized obstacles. This last calculation is limited only by the numerical precision of the computer and allows us to study the escape transition for finite chains via a procedure that is essentially exact. This and the other approaches of the paper show that a jump in the force profile does occur with compression.

II. TWO-STATE MODEL AND THE EFFECT OF FLUCTUATIONS

We consider a chain of N statistical monomers, each of size a. The chain is ideal, end-tethered to a grafting plane, and has a natural size that scales as $aN^{1/2}$. We impose a finite-sized disk of radius L, larger than the size of the chain but smaller than the elongated dimension of the chain, aN, centered over the grafting point of the chain. The separation distance between the obstacle and grafting surface is H. As H is decreased, the chain is compressed and we refer to H as the compression distance. If the radius is sufficiently large, we can consider all chain configurations to be partitioned into two distinct states: imprisoned and escaped.

The free energy of the imprisoned chain, confined wholly between the plane and compressing cylinder is [6] $F_{imprison}/k_BT = Na^2/H^2$, where here, and in the remainder of the section we neglect numerical prefactors. The free energy of an escaped chain is comprised of the compression energy of m monomers in the tethered umbilical, ma^2/H^2, and the stretching penalty of the umbilical, stretched to the edge of the cylinder, $L^2/(ma^2)$. Those monomers that have escaped from underneath the cylinder suffer a negligible free-energy penalty. Under thermodynamic equilibrium, the chain will shuffle or readjust the number of monomers in the tether so as to minimize its energy, and consequently, the energy of the escaped state is $F_{escaped}/k_BT = 2L/H$. In the previous theoretical treatments, the chain fluctuates within each state; however, at a given compression the chain always resides in the state of lowest energy. That is, the population of each state is quantized, being either 1 or 0. At weak compressions, or large H, the imprisoned state has lower energy, $F_{imprison} < F_{escape}$ and all chains are imprisoned. As the chain is compressed, or H reduced, the imprisoned state energy increases until at a critical compression, $H^* = Na^2/2L$, the energy of the two states are identical, $F_{imprison} = F_{escape}$. As the chain is compressed beyond H^*, the system jumps suddenly from one state to the other. Across this jump, the free energy is constant, but the radial size of the chain and the force transmitted to the obstacle are discontinuous. This two-state model, without fluctuations between states, is the basis of the early theory papers [6–9]. However, near the transition the difference in the energy between the states is small (of order k_BT), and hence, both states will be populated to a substantial degree. The transition will thus often be more gradual than that suggested in the early theory papers and in accordance with recent simulation studies.

We can extend the two-state model to include fluctuations between states, allowing both states to be simultaneously populated at any given compression. In the usual kind of experiment, where one has only a single chain compressed under a single obstacle this means that the chain spends a certain fraction of its time imprisoned and the remainder of its time escaped. It is of course also possible to imagine many chains, each compressed under an obstacle with a fraction of the chains escaped. In the compression case we simply have a two-state system in which each state can be populated, much like the simple two-state models of atoms ubiquitous in atomic physics courses.

The mixing between the two states can be estimated by the partition function, written as $Z = \exp(-F_{escape}/k_BT) + \exp(-F_{imprison}/k_BT)$. This is not an exact representation of the partition function as it ignores some prefactors associated with the relative phase space volumes of the two states; however, it is a reasonable representation in the spirit of the two-state model. The free energy of the total system is then $F = -k_BT \ln Z$ and the force exerted by the chain on the obstacle is

$$f = -\frac{\partial F}{\partial H} = 2k_BTLH^{-2}(2H^*/H + g)/(1+g), \qquad (1)$$

where $g \equiv \exp[-2LH^{-1}(1-H^*/H)]$. This force law changes from $f = 4k_BTLH^*H^{-3}$, at $L \gg H \gg H^*$ to a weaker force law, $f = 2k_BTL/H^2$, for compression distances $H \ll H^*$. How sharply this crossover occurs as H is varied through H^* depends upon the function g, which is just the relative population of the two states. In particular, g must change rapidly near $H = H^*$ in order for the transition to be sharp. Examining g it is clear this will occur when the obstacle radius is much larger than the critical height, $L/H^* \gg 1$ or equivalently when $L \gg N^{1/2}a$; that is, when the disk radius is much greater than the unperturbed chain size.

Figure 1(a) is a scaled plot of the force profiles, predicted from Eq. (1), versus the compression distance for three difference obstacle radii. It is clear that for an obstacle of dimensionless radius $L/H^* = 100$, compression leads to an escape transition that is very sharp, and that for smaller obstacles, as for example $L/H^* = 10.0$, a transition is still evident, although it is less sharp. For an obstacle of dimensionless radius $L/H^* = 2.0$ the escape transition has almost disappeared. In general, for a reasonably sharp transition we require obstacles of large radius, $L/H^* > 10$, in agreement with recent simulation results [13,14]. These force curves are also reminiscent of those obtained in previous computer simulations [10–12].

This two-state technique can also be used to calculate the radial size as well as the maximum extent of the chain in the vertical direction (or its height), for the system. The average maximum radial extent for the chain is

$$\langle R_{max} \rangle = (1+g)^{-1}(\sqrt{2LH^*} + gL + g\sqrt{2LH^* - HL}), \qquad (2)$$

while the average maximum extent in the vertical direction is

$$\langle z_{\max} \rangle = (1+g)^{-1}(H + g\sqrt{2LH^* - HL}). \qquad (3)$$

These expressions are obtained from the expected size of a confined random walk, and the escaped random walk, weighted by the relative populations in each case. Figures 1(b) and 1(c) are plots of the maximal radial size and maximal height, respectively, versus the compression distance.

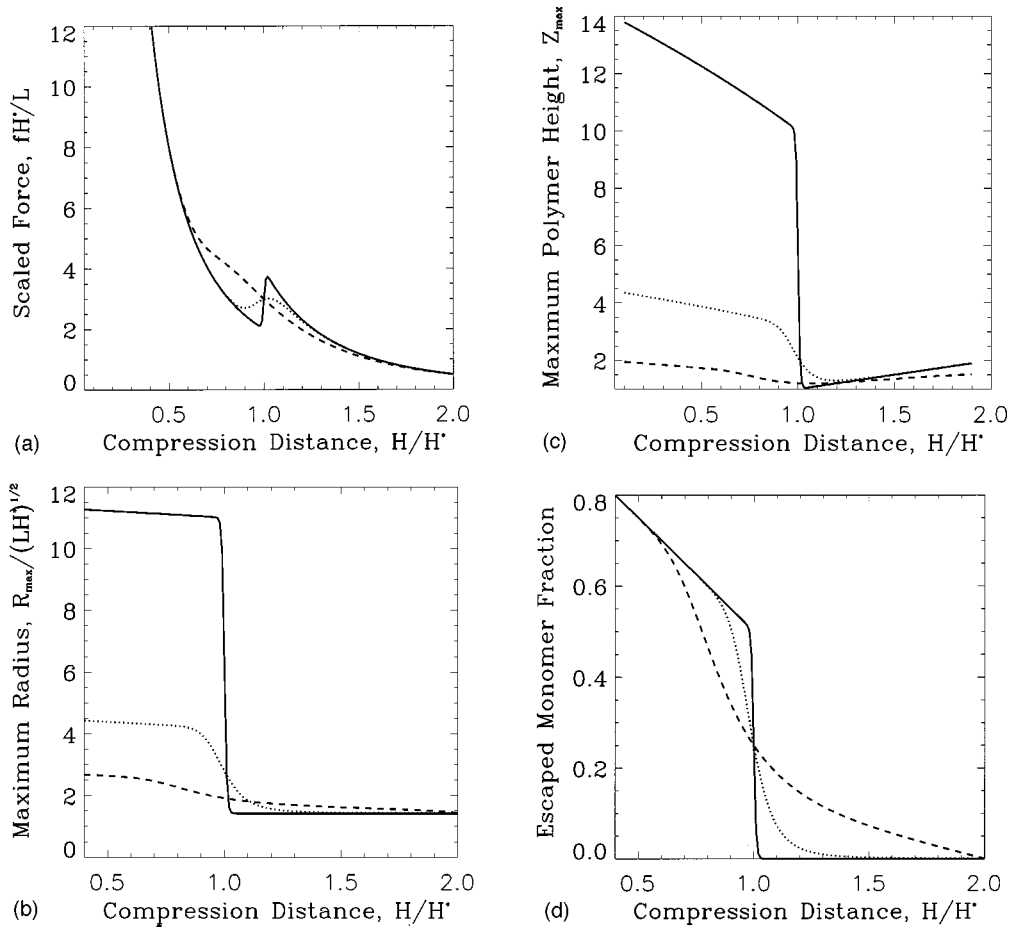

FIG. 1. Predictions of the two-state model with fluctuations for a cylinder of radius L compressing an end-tethered chain against a grafting plane at variable compression distance H. Predictions are shown for cylinders of three different dimensionless radii: $L/H^*=100$ shown in solid lines, $L/H^*=10$ in dashed lines, and $L/H^*=2$ in dotted lines. The compression distance, or the height of the slit between obstacle and grafting plane, is scaled by the critical compression distance, H^*. The predicted quantities versus compression distance are (a) force, in units of kT/H^* and scaled by L/H^* (b) maximal radial extent of the chain, scaled by $\sqrt{LH^*}$, (c) maximal height of the chain, scaled by yL/H^*, and (d) fraction of monomers that have escaped from underneath the obstacle. In each of these, the escape transition is marked by sharp changes in the measured quantities at $H/H^*=1$ whenever the obstacle radius is large, i.e., $L/H^*=100$. But when the obstacle radius is smallest, $L/H^*=2$, the measured quantities change gradually with compression distance, and the sharp transition has disappeared.

These mirror what is seen in simulations, but again the transition only becomes sharp when g changes rapidly, i.e., when the obstacle radius is sufficiently large, $L/H^*>10$. Finally we can calculate the fraction of monomers escaped from under the obstacle. This is

$$\langle N_{escaped}/N\rangle=[1-H/(2H^*)]g/(1+g) \tag{4}$$

and is plotted in Fig. 1(d) versus compression distance. Again, we see that the fraction of escaped monomers changes nearly discontinuously for large obstacle radii and more gradually for smaller obstacles.

This two-state model is, of course, approximate. But it provides descriptions that are comparable to simulation and it allows us to understand the results simply in terms of two states. A more rigorous approach is to evaluate the complete partition function of the chain, explicitly including all degrees of freedom of the chain. This is done in the following two sections, where we evaluate the partition function stochastically and numerically.

III. STOCHASTIC EVALUATION OF THE PARTITION FUNCTION

A common technique used in statistical mechanics for the evaluation of partition function and associated averaged quantities is to generate configurations stochastically on a computer. Since the initial theoretical studies [6–9], a number of these computer simulations have appeared in the literature [10–14]. All of these have been stochastic simulations that generate configurations of chains end-tethered underneath a cylindrical obstacle using the Metropolis Monte Carlo method. In this method, successive configurations are constructed through biased, local moves of monomers within the chain. This method can be time consuming as the relaxation time (or Rouse time) for a chain of N monomers scales as N^2. Thus many local weighted monomer moves must be made to generate a large number of chains with independent configurations. Moreover, there can be a significant ($>k_BT$) energy barrier between the imprisoned and escaped states, which may further frustrate the Metropolis sampling of configurational space. This barrier arises from the extra energy needed to stretch the chain to the edge of the cylinder

so that at least one monomer can escape and becomes more significant as the radius of the obstacle is made larger [6–8].

However, if the chain is ideal and modeled as a random walk, then we can generate independent configurations successively and in an unbiased way, sampling configuration space uniformly. Under high compression, severe entropic barriers restrict the sampling of configurations; however, information can be gleaned cheaply at moderate compression. The partition function for such a chain in the presence of hard walls is $Z_N(H)=\Sigma_{\text{all configurations}}\exp(-U/k_BT)$, where the sum is over all possible configurations of the end-tethered chain of N monomers. Since the walls are infinitely hard and monomer-monomer interactions are absent, this sum reduces to the sum over all allowed chain configurations, each of equal weighting, i.e., $Z_N(H)=$number of allowed configurations. By ''allowed configurations'' we mean those that do not penetrate or intersect the grafting plane or compressing obstacle. The Helmholtz free energy is $F=-k_BT\ln Z_N(H)$, and all of the averages in the system can be calculated by averaging over the configurations.

We implement this using a more symmetrical geometry than the grafting plane and compressing disk of the previous section. Instead, we take two cylinders, each of radius R, whose flat ends are separated by a distance H. A chain is placed in the space between the flat ends of the cylinders, with its end centered and fixed midpoint between the cylinders. We construct each chain by ''growing'' it from the first fixed monomer on a cubic lattice. Each consecutive monomer is placed discretely and randomly in one of the six cubic lattice sites lying adjacent to the previous monomer's lattice site. If at any point, the chain collides with one of the cylinders, then that configuration is rejected and we begin growing a new chain. An allowed configuration is a random walk of N cubic lattice steps which does not intersect the cylinders. Of course we cannot generate all of the allowed configurations in this way; there are simply too many. However, since the free energy is only defined up to a constant it is clear that we can replace the partition function defined above by a new partition function $Z'_N(H)\equiv Z_N(H)/Z_N(\infty)$, which is simply the fraction of random walks (out of all possible random walks) that do not penetrate the walls. We can estimate this by making T attempts at generating a random walk so that $Z'_N(H)=Q/T$, where Q is the number of successful random walks, that is random walks of N steps which do not penetrate the boundaries. Provided our number of attempts is large, the quantity $F=-k_BT\ln(Q/T)$ is a good approximation to the free energy. Moreover, our successful random walks represent an unbiased sample of the chain configurations over which we can construct descriptive averages, such as the average maximal radial extent of the chain and the average maximal height of the chain.

It is important to ensure that we have constructed an adequate sampling of configuration space such that the fraction of successful walks, Q/T, is representative of the entire configurational space of the chain. First, we can fix T, the number of attempted chain growths and count the number of successful random walks, Q. This has the advantage that at very high compression almost all of the walks we start terminate after only a few steps and the program becomes very fast at high compressions. However, if the number of successful walks, Q, is small, then the sampling of the configurational space may be inadequate. Instead we can fix Q and increase T until we get enough successes. This reduces the scatter at high compressions, but tends to increase it at weak compressions where the configurational space is larger and chain configurations can vary more widely. We found that a combination of these two techniques gives the best results. For a chain of $N=10\,000$ monomers, we ensure that we have at least 5000 successful random walks, as well as at least 10 000 attempted walks. This produces reasonable sample sizes and averages. However, the minimum number of successful random walks becomes insufficient and very difficult to obtain at very small compressions where successful random walks become very rare. At such high compression it is necessary to bias the sampling technique, which we do not do here.

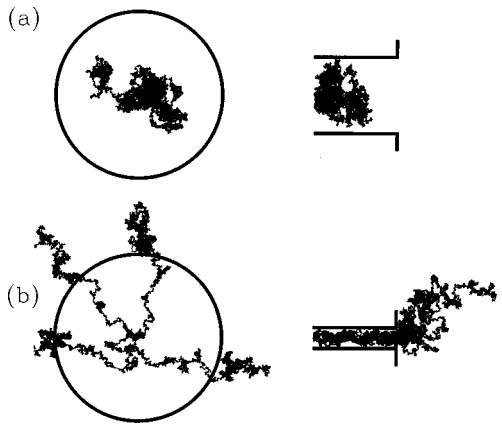

FIG. 2. Configurations of chains with $N=10^4$, constructed on a cubic lattice with one end tethered centrally at the midpoint between the flat ends of two cylinders of radius $L=120$ lattice units and separated a distance H. Shown are the top and side views where the transparent cylinders are in (a) weak compression, $H=110$ units, and (b) strong compression, $H=30$ lattice units. Each view contains four chain configurations, each generated independently as a random walk starting from the fixed tether. The four chains in the side views have been rotated such that their end-to-end vectors are coincident, i.e., we plot their (r,z) monomer coordinates where $r=\sqrt{x^2+y^2}$. In this figure, a random number ϵ, uniformly distributed on $[-0.5,0.5]$, has been added to the discrete monomer positions to enhance the images.

This stochastic method allows us to generate many lattice-based chains, confined between the flat ends of cylinders of radius $L=50$, 120, and 1000 lattice units and separated a variable distance, H, apart. Figure 2 shows four typical chain configurations from both top and side views, sandwiched between two cylinders, at weak compression or $H=110$ lattice units, and at strong compression or $H=30$ units. Note that the weakly compressed chains are imprisoned: they are barely distorted from their isotropic trajectories. However, the strongly compressed chains have escaped through the formation of highly stretched, and radially oriented umbilical tethers. These chains, along with at least 5000 others generated at each specified compression distance are used to construct averaged chain properties, namely, the chain's free energy, maximal radial extent, and maximal height, as a function of compression.

Figure 3(a) is the average maximal height of the chain, measured as the distance from the tethered end, located at the

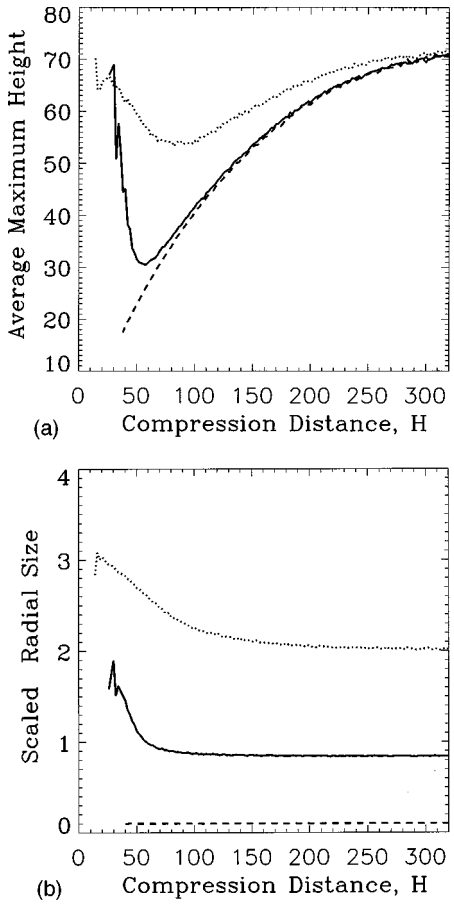

FIG. 3. Average properties for a $N=10^4$ monomer, lattice-based chain whose end is centrally placed at the midpoint between the flat ends of two cylinders, separated a variable distance H. The averages are constructed from an ensemble of random walks of N steps on a cubic lattice which do not intersect the compressing cylinders and plotted against the compression distance, H. For most compression distances investigated, the average was constructed from at least 5000 successful chain configurations. The average properties are shown for cylinders of three different radii: $L=1000$ shown by the dashed line, $L=120$ by the solid lines, and $L=50$ by the dotted line L measured in monomer units a. The averaged quantities versus compression distance are (a) maximal height, and (b) maximal radial extent divided by obstacle radius, L. These figures show that the average chain confined between cylinder of radius $L=120$ undergoes an escape transition. The average size of the $N=10^4$ chains is larger than the cylinders of radius $L=50$ and consequently, there is no sharp escape transition. The cylinders of radii $L=1000$ are effectively infinite in size with respect to the chain size as the chains are completely confined between the cylinders, deforming uniformly with compression and exhibiting no escape transition under the compressions studied.

central midpoint between the cylinders, to the monomer furthest removed from the plane which bisects the gap between the cylinders. A chain height that exceeds the compression distance H is neither a necessary nor sufficient condition for escape. However, a minimum in the average maximal chain height is indicative of nonuniform deformation within the chain. With compression, the height of the confined portion of the chain is squeezed and its height decreases; however, the escaped portion of the chain expands as more monomers of the chain are squeezed out from between the cylinders at strong compression. Thus, an average height that decreases monotonically with compression is associated with a completely trapped chain that does not escape, as in $L=1000$ of Fig. 3(a). A height that decreases identically with large obstacles at weak compression, and then sharply increases is indicative of an escape transition, as in the $L=120$ case. Note that in the case of the $L=50$ cylinders, the average height of the weakly compressed chain is larger than that of a chain confined between cylinders of $L=120$ and 1000 at the same compression. The chain height is not as dramatically reduced by the compressing cylinders as in the case of larger cylinder radii. This is indicative of cylinders of radii smaller than the natural size of the chain. The chain does not escape with compression, there is no escape transition, and the nonuniform deformation of the chain, while still evident, is not as pronounced as that in the cases where escape transitions occur.

Figure 3(b) is the average maximal radial extent of the chain, versus compression distance. When the maximal radial position exceeds the radii of the cylinders, then we can state that, on average, a portion of the chain is outside the radius of the cylinders. Thus, chains that are trapped between cylinders of radii $L=50$ and $L=1000$ do not exhibit escape transitions as the radial extent scaled by L does not trespass unity with compression. However, the averages indicate that chains trapped between cylinders of $L=120$ do undergo an escape transition.

Figures 4 and 5 show different chain configurations at specified L and H and allow one to see average chain shape and monomer density. Note that the quantitative results obtained from stochastic evaluation of the partition function are, with one exception, very similar to those in the approximate two-state model with fluctuations (Sec. II). The exception is that the stochastic method cannot reliably access the strongly compressed region, where the maximum chain dimensions (height and radial extent) are expected to plateau.

IV. EXACT NUMERICAL EVALUATION OF THE PARTITION FUNCTION

The stochastic generation of random walks does not allow us to construct the free energy to the precision that is required to construct force profiles, particularly at intermediate to strong compression. An alternative approach is to consider an ideal chain with a ''spring'' or bonded potential which is specifically selected such that the partition function and associated properties can be solved analytically. Here we select the bonded potential between monomers i and $i+1$ to be of the form [16]

$$k(|x_{i+1}-x_i|+|y_{i+1}-y_i|+|z_{i+1}-z_i|), \tag{5}$$

where the coordinates of monomer i are given by (x_i,y_i,z_i). This potential has the peculiar property that the force between the two monomers is constant and the energy increases as their separation increases. The form of this potential implies that the chain is not quite spherically symmetric in bulk, but this asymmetry disappears as N^{-1}. Indeed, a chain of N such monomers becomes Gaussian as N increases and the properties of the chain will be independent of the exact form of the bonding potential except on the scale of the monomer-monomer separation. The average separation, a,

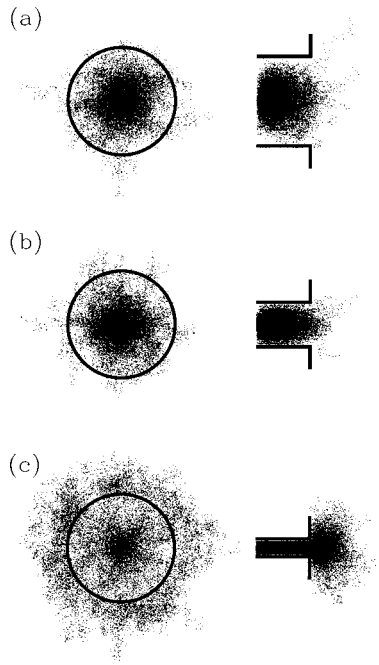

FIG. 4. Snapshots of 200 lattice-grown chains, each of $N=100$ monomers, compressed between two transparent cylinders of radii $L=12$ separated a variable distance H. Each point corresponds to the location of a monomer and collectively describes the expected density of monomers. We have added a random number ϵ, uniformly distributed on $[-0.5, 0.5]$, to the discrete monomer positions to enhance the images. Side and top views are given for three different compression distances: (a) $H=20$, (b) $H=10$, and (c) $H=4$. In (a) we have weak compression and the monomers are mainly located near the center of the circle. The monomer density is largest at the center, because the first monomer is always located at the center $r=0$ and the density decreases with r as the number of possible monomer positions scales as r. In (b) the chain is more compressed and has expanded slightly, but is still rarely escaped. In (c) escape has occurred. There is still a central dense region, although this is much reduced in size. This is surrounded by a less dense region, followed by a more dense halo of escaped monomers outside the circle.

between bonded monomers is $a^2=6(k_BT/k)^2$; the average end-to-end distance is $a\sqrt{N-1}$; and the radius of gyration, R_g, is given by $R_g^2=(N-1/N)a^2/6$. The use of such a bonding potential for force calculations in a slit has been thoroughly examined in an earlier paper by one of the authors [16].

We can construct an analytic expression for the partition function of such a chain, end-tethered and compressed between finite obstacles. The obstacle geometry is similar to that of Sec. III, except that we reduce the dimension of the problem from 3 to 2. This reduction in dimension is necessary only to keep the complexity of the analytic solution minimal. We thus consider compression of a chain between two rectangles. The $i=1$ monomer is fixed at the (x,z) origin, selected to be radially centered and midpoint between the two obstacles. The two impenetrable obstacles exclude monomers from the regions $|x|<L$, $z>H/2$ and $|x|<L$, $z<-H/2$, so that the compression distance or slit separation is H and the half-width of the obstacle is L. Thus the two dimensional version of the problem is equivalent to a three dimensional problem in which the obstacles extend indefinitely in the y direction.

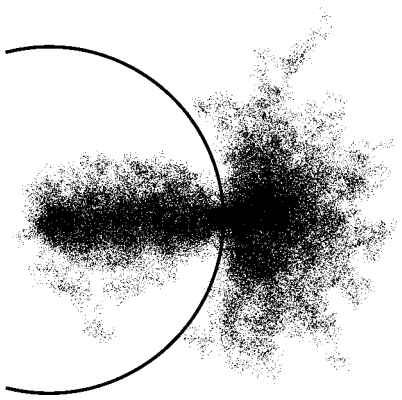

FIG. 5. Snapshots of 98 chains, each of $N=1000$ monomers compressed between two transparent cylinders of radius $L=40$ that are separated a distance $H=10$ apart and viewed from the top of the cylinders. We have added a random number ϵ, uniformly distributed on $[-0.5, 0.5]$, to the discrete monomer positions to enhance the images. These chains represent the subset of chains which have escaped, i.e., those which have at least one monomer outside of the cylinder radii. We have also rotated each chain so that the first escaped monomer of all chains is located at a prescribed point. This allows us to discern the average shape of the chain from the monomer density. It is clear that the imprisoned monomers form a highly stretched tether and the escaped monomers form a fairly isotropic random walk.

The partition function for the chain is then given by

$$Z(H)=\int_{A_2}\cdots\int_{A_N}\exp\left(-\beta k\sum_{i=1}^{N-1}(|x_{i+1}-x_i|+|z_{i+1}-z_i|)\right)\prod_{i=1\ldots N}dz_i dx_i, \tag{6}$$

where A_i is the allowed area for monomer i (i.e., all area apart from $|x_i|<L$ and $|z_i|>H/2$), and $\beta=1/(k_BT)$. If one starts to evaluate the x and z integrals in Eq. (6), progressing through each of the monomers beginning with $i=2$, the structural form of the solution becomes apparent. After the coordinates of monomer i have been integrated out, the terms of the resulting expression are all of the form $\exp(\pm\beta k|x_{i+1}|\pm\beta k|z_{i+1}|)|z_{i+1}|^n|x_{i+1}|^m$ multiplied by coefficients that depend on H and L, and where m and n are integers between 0 and $i-2$. These coefficients can be expressed in recurrence relations, which in turn can be used to obtain analytic results for $Z(H)$ and its derived quantities such as compressive force. The detail of this algebraically complicated procedure and the resulting expressions are given in the Appendix.

We can evaluate the partition function, and its derivative with respect to H, as functions of H, L, and a by iteratively evaluating the recurrences for finite N using a mathematical algebra package. However, this requires $O(N^4)$ storage, and becomes impractical with large number of monomers, N. A more efficient implementation is to fix the values of H and L, and evaluate the recurrences numerically. This requires $O(N^4)$ time but only $O(N^2)$ storage. A simple FORTRAN90 code to perform this evaluation is available from the authors [17]. The main limitation of the numerical scheme is due to the finite precision of computer arithmetic. The region of

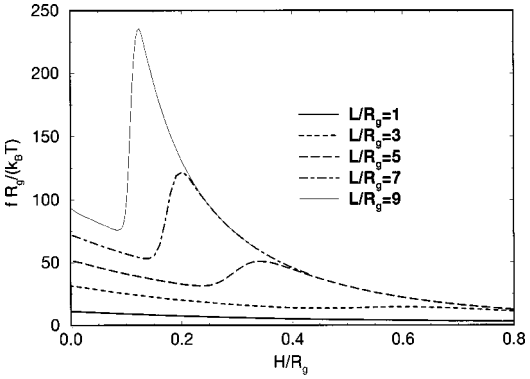

FIG. 6. Force f as a function of compression distance H for a chain with $N=40$ monomers in the two-dimensional compression problem, using the numerical evaluation of the exact result. Thick solid line, obstacles half-width $L=R_g$; dashed line, $L=3R_g$; long dashed line, $L=5R_g$; dotted-dashed line, $L=7R_g$; thin solid line, $L=9R_g$.

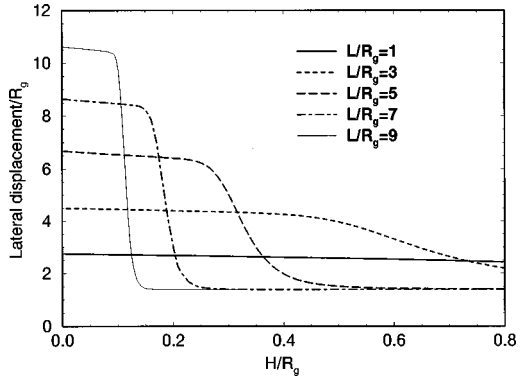

FIG. 7. RMS lateral distance of the end monomer of the chain from the anchoring point for $N=40$, as a function of separation, H. Curves as in Fig. 6.

most interest in the problem is for $H \ll R_g$, and as N increases there is a growing loss of precision. In ordinary double precision arithmetic, this limits N to about 40, depending somewhat on the value of L. This can be extended up to around $N=100$ using quadruple precision, but at the cost of a significant increase in computation time.

From the partition function, we can evaluate the analytic compressive force $f(H)=-1/Z\,\partial Z(H)/\partial H$. Figure 6 shows the force, f, as a function of the compression distance, H, for chain with $N=40$ monomers and various values of L. For $L/R_g=1$ the force is monotonically increasing as H decreases. For $L/R_g=3$ there is a broad local maximum, and for larger values of L this local maximum becomes sharper, and occurs at stronger compression or smaller H. This characteristic shape of the force profile near the escape transition is in accord with the predictions of the two-state model discussed in Sec. II. As H tends to 0, the force tends to a finite value for these $N=40$ chains. This is an artifact of the spring potential and the finite number of monomers; i.e., by applying large enough pressures it is possible to squeeze all the monomers (other than the anchoring one) out of the slit. A finite-sized chain with finitely extensible or inextensible bonds would give a divergent force at small separations. However, the flexible bond potential in Eq. (5) used in a chain with large N will also yield a divergent force at high compression.

The coefficients that are found in the evaluation of the partition function can also provide the analytic description of the location of the free chain end or $i=N$ monomer. Here we look at the root-mean square displacement of the $i=N$ monomer from its tethered $i=1$ end as a function of compression. It is instructive to look at the lateral or x-displacement separately from the vertical or z-displacement and note how each of these shows the signature of the escape transition. The root-mean square (rms) average x displacement is shown in Fig. 7 as a function of compression distance H and for the same range of obstacles widths L as in Fig. 6, again for $N=40$. As the chain is compressed to a separation H of $O(1/L)$, the chain escapes, and the average lateral displacement increases. This transition becomes sharper as the obstacle size, L, increases. Comparing Figs. 6 and 7, we see that the separation at which there is a transition in lateral displacement corresponds to a local maximum in the force. Note that for the escaped chain, the rms average extent is about $1.6R_g$ beyond the edge of the slit. Since the problem considered in this section is two dimensional, one can think of the escaped chain as being like a chain anchored at one end to an impenetrable, vertical wall (the anchoring point being where the chain emerges from the slit). This analogous problem is easily solved in the long chain limit, and in that case the rms average of the lateral component is $2R_{esc}$ normal to the wall, where R_{esc} is the radius of gyration of the part of the chain that has escaped. In this case the flexibility of the bond potential means that for small H, $R_{esc} \approx R_g$.

If one examines the rms average of the vertical component (in the z direction) of the end monomer displacement, then there is a similar transition, as shown in Fig. 8. If the obstacle is large, i.e., $L \gg R_g$, then for weak compressions, or $1/L \ll H \ll L$, there is a decrease in chain ''height'' as the chain is compressed. When compressed at a critical H, which is $O(1/L)$, then the chain can escape and spread out in the vertical direction. Note that at strong compression or small separations, the rms average of the z-component is about $1.4R_g$. Using the analogy discussed above with a chain attached to a wall, in the long chain limit the rms average of the vertical component is $\sqrt{2}R_{esc}$.

It is also possible to examine the distribution of the position of the end monomer, and not just the RMS average.

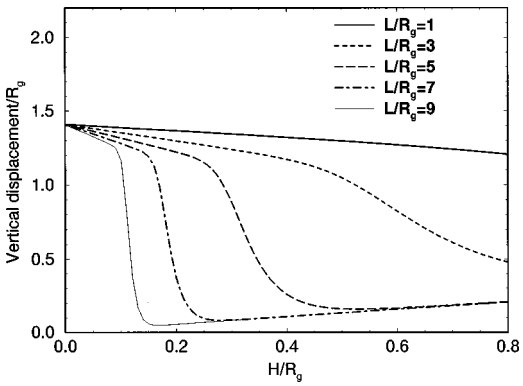

FIG. 8. RMS vertical distance of the end monomer of the chain from the anchoring point for $N=40$ as a function of separation, H. Curves as in Fig. 6.

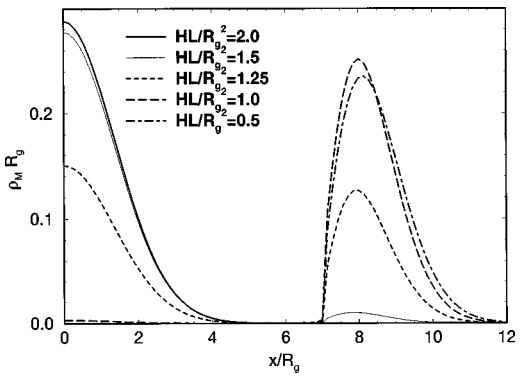

FIG. 9. Distribution of the lateral position of the end monomer from the anchoring point for $N=40$ and $L=7R_g$. Thick solid line, $HL/R_g^2=2.0$; thin solid line, $HL/R_g^2=1.5$; dashed line, $HL/R_g^2=1.25$; long dashed line, $HL/R_g^2=1.0$; dotted-dashed line, $HL/R_g^2=0.5$.

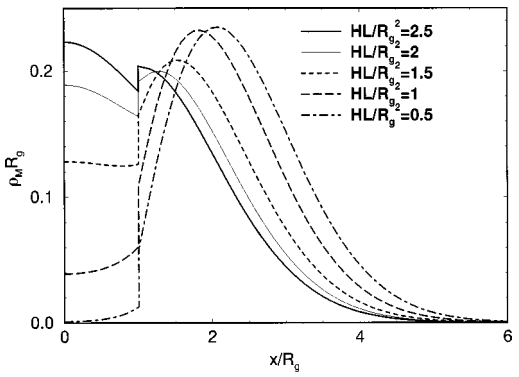

FIG. 11. Distribution of the lateral position of the end monomer from the anchoring point for $N=40$ and $L=R_g$. Thick solid line, $HL/R_g^2=2.5$; thin solid line, $HL/R_g^2=2$; dashed line, $HL/R_g^2=1.5$; long dashed line, $HL/R_g^2=1.0$; dotted-dashed line, $HL/R_g^2=0.5$.

Again, it is instructive to look at the lateral and vertical components of the distribution separation. Figure 9 shows the distribution in the lateral direction for $N=40$, $L=7R_g$ and five different separations, corresponding to $HL/(R_g)^2=0.5$, 1.0, 1.25, 1.5, 2.0. The area under each of the curves is 0.5, since the distribution is symmetric about $x=0$. At the largest separation, the end monomer is almost entirely confined to the slit. When $HL/(R_g)^2=1.5$, corresponding roughly to the location of the local maximum in the force, there is a small proportion of ends outside the slit, and as H is decreased further, this proportion grows rapidly, until at $HL/(R_g)^2=0.5$ almost no ends remain in the slit. The distribution of ends outside the slit in the lateral direction resembles that for a polymer anchored to a flat wall, as per the analogy discussed above.

The corresponding distribution of chain ends in the vertical direction is shown in Fig. 10, again for $N=40$ and $L=7R_g$. The main graph shows the distribution for ends outside the slit ($|x|>L$), while the inset shows the distribution of ends inside the slit ($|x|<L$). For $HL/(R_g)^2=2.0$ and 1.5, most of the chain ends are still confined in the slit, where the density is increasing as H decreases. As H is reduced further, the chain begins to escape, the density of chain ends in the slit falls rapidly, and the proportion of chain ends outside the slit rises. Again the distribution of ends outside the slit resembles the distribution of ends in the lateral direction for a polymer anchored to a flat wall.

Having examined the distribution of the end monomer for the case when $L \gg R_g$, it is instructive to look at the distributions for $L=R_g$ and $N=40$. In this regime we expect that significant numbers of monomers will have escaped from under the obstacle, even for the case of no compression. Figure 11 shows the lateral distribution and Fig. 12 the vertical distribution for a set of separations which correspond to $HL/(R_g)^2=0.5$, 1, 1.5, 2, 2.5. Here is it evident that even at large separations, the chain ends penetrate well beyond the edge of the slit. Note that the density distribution is continuous in x and z, and the discontinuity evident in the lateral direction in Fig. 11 at the edge of the slit arises because of the integration over the vertical direction. As the separation decreases, the chain ends are gradually squeezed out of the slit, but there is no sharp transition. Observing the distribution in the vertical direction in Fig. 12, it is interesting to note that the spread of monomers outside the slit initially decreases as H decreases, as the reduction in slit width restricts the z displacement of the point where the chain can first escape.

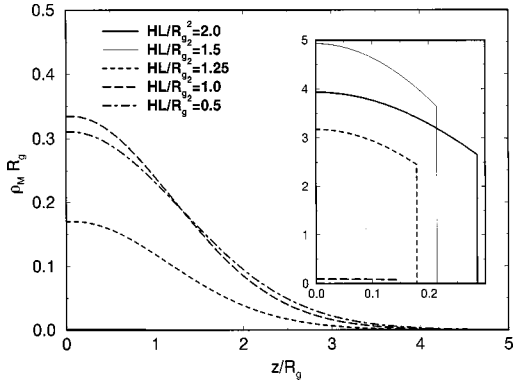

FIG. 10. Distribution of the vertical position of the end monomer from the anchoring point for $N=40$ and $L=7R_g$. Curves as in Fig. 9. The main graph shows the distribution for the case where the end monomer is outside the slit ($|x|>L$) and the inset shows the distribution when the end monomer is inside the slit ($|x|<L$).

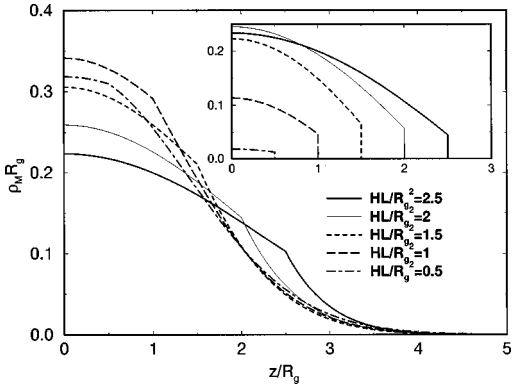

FIG. 12. Distribution of the vertical position of the end monomer from the anchoring point for $N=40$ and $L=R_g$. Curves as in Fig. 11. The main graph shows the distribution for the case where the end-monomer is outside the slit ($|x|>L$), and the inset shows the distribution when the end monomer is inside the slit ($|x|<L$).

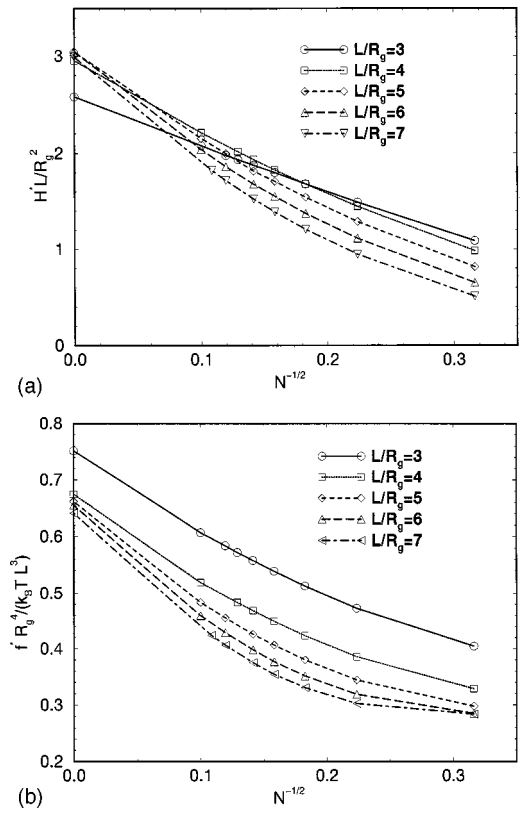

FIG. 13. Extrapolation of scaled critical compression and critical force to the long chain limit, for various values of the obstacle half-width, L/R_g. The symbols give the values obtained from an exact numerical evaluation of the partition function for finite chains with up to $N=100$ monomers. The symbols at 0 on the horizontal scale are the extrapolated values from a least squares fit of a quadratic in $N^{-1/2}$, while the curves are only a visual guide. Solid line and circles, $L/R_g=3$; dotted line and squares, $L/R_g=4$; dashed line and diamonds, $L/R_g=5$; long dashes and triangles, $L/R_g=6$; dotted-dashed line and inverted triangles, $L/R_g=7$. (a) Scaled critical compression H^*L/R_g^2, (b) scaled critical force $f^*R_g^4/(k_BTL^3)$.

The force curves obtained for $N=40$ show the qualitative features predicted by the two-state model, in particular the existence of a local maximum and minimum in the force versus separation curve for large enough values of L. However, 40 monomers is still not a long chain and the scaling behavior expected in H^* is not yet evident. By doing a series of calculations at a fixed value of L/R_g with values of N up to 100, we can extrapolate to the large N limit, where the results should be independent of the specific monomer-monomer potential employed. We can then examine how the critical compression, H^*, and force, f^*, at the local maximum in the force curve scale with L. The two-state model predicts that H^*L/R_g^2 and $f^*R_g^4/(k_BTL^3)$ should be constant for large enough L.

Figure 13(a) shows the numerical values of H^*L/R_g^2 for $L/R_g=3,\ldots,7$ and N up to 100, plotted on a scale of $N^{-1/2}$, along with the extrapolated points for large N (these are the points at zero on the horizontal scale). The extrapolation is done by a least squares fit of a quadratic in $N^{-1/2}$, in order to capture the upward curvature of the data for fixed L and increasing N. As L increases, the extrapolated points for large N appear to reach and maintain a constant value of $H^*L/R_g^2\approx 3.0\pm 0.1$, allowing for some uncertainty in the extrapolation. The extrapolated value for $L/R_g=3$ is clearly lower than the others, since this is in the region where the transition first appears, and the local maximum in the force is broad.

Figure 13(b) similarly shows the numerical values of $f^*R_g^4/(k_BTL^3)$ and the extrapolation to large N. As L increases, the extrapolated values appear to be approaching a constant value of $\approx 0.65\pm 0.03$, although the convergence with L is slower than in Fig. 13(a). In both of these graphs, it is clear that fixing N and varying L gives misleading results as far as the scaling predictions for large L are concerned, since the rate of approach to the large N limit varies with L. By first extrapolating to large N we have been able to confirm the quantitative validity of the predictions of the two-state model as L varies.

V. CONCLUSIONS

In this paper we have studied in some detail the compression of an ideal chain between one or two finite obstacles. Three different methods and three different geometries have been used, but in all cases we find evidence of an escape transition, as predicted by earlier simple theories [6–9]. We have shown how thermal fluctuations near the transition can blur what was previously a sharp transition. Most importantly we have provided an exact calculation of the partition function, which shows unambiguously that a maximum and minimum occurs in the force curves as a function of compression. This calculation is in many ways vital, since it is in principle exact, and overcomes all of the difficulties and inherent uncertainties associated with the earlier theories and computer simulations. It also lays to rest claims that have occurred in a number of unpublished works, that there is no jump in the force curve under compression. We note in concluding that our results are valid for the case where the height is the independent variable, and where the force (and other quantities) are measured for a given height. In this case the Helmholtz free energy is the appropriate thermodynamic potential, and there is a jump in the force at the transition. Other situations can also be realized. For instance, it is possible to have force as the independent variable and measure the height. In this case the Gibbs free energy is the appropriate potential and then one gets a jump in the height as a function of force [15].

ACKNOWLEDGMENTS

D.R.M.W. acknowledges support from an ARC QEII. The authors of Refs. [13,14] are thanked for providing their information prior to publication.

APPENDIX

The exact evaluation of the partition function given in Eq. (6) (and its derivative) for a finite chain of N monomers proceeds as follows. It is convenient to scale the lengths by $1/(\beta k)$, so that the new monomer positions are given by $x_i^{new}=\beta k x_i^{old}$, etc. The dimensionless half-width of the obstacles is then given by $\hat{L}=\beta kL$, and the dimensionless half-separation by $\hat{H}=\beta kH/2$. Thus the two obstacles now oc-

cupy the regions $|x|<\hat{L}$, $z>\hat{H}$ and $|x|<\hat{L}$, $z<-\hat{H}$.

One begins the integrals at the fixed end of the polymer ($i=1$). After the coordinates of monomer $i-1$ have been integrated out, the expression is a function of z_i and x_i, and has the following form. For $|z_i|<\hat{H}$ and $|x_i|<\hat{L}$, the form is

$$\sum_{n=0}^{i-2}\sum_{m=0}^{i-2}|z_i|^n|x_i|^m[A^i_{nm}\exp(-|z_i|-|x_i|)+B^i_{nm}\exp(|z_i|-|x_i|)+C^i_{nm}\exp(-|z_i|+|x_i|)+D^i_{nm}\exp(|z_i|+|x_i|)].$$

For $|z_i|<\hat{H}$ and $|x_i|>\hat{L}$ the form is

$$\sum_{n=0}^{i-2}\sum_{m=0}^{i-2}|z_i|^n|x_i|^m[E^i_{nm}\exp(-|z_i|-|x_i|)+F^i_{nm}\exp(|z_i|-|x_i|)].$$

For $|z_i|>\hat{H}$ and $|x_i|>\hat{L}$ the form is

$$\sum_{n=0}^{i-2}\sum_{m=0}^{i-2}|z_i|^n|x_i|^m[G^i_{nm}\exp(-|z_i|-|x_i|)].$$

To perform the next integration in the partition function, these expression are multiplied by $\exp(-|x_{i+1}-x_i|-|z_{i+1}-z_i|)$ and integrated over A_i. Collecting terms, the resulting expression is again of the above form, and the new coefficients A^{i+1}_{nm}, B^{i+1}_{nm}, etc. obey the following set of recurrence relations. To reduce the length of the formulas, common subexpressions are written as f_q for some integer q, and these f_q expressions are given below after the recurrences,

$$A^{i+1}_{0,0}=\sum_{n=0}^{i-2}\sum_{m=0}^{i-2}(A^i_{nm}f_1f_2+B^i_{nm}f_3f_2+C^i_{nm}f_1f_5+D^i_{nm}f_3f_5+E^i_{nm}f_1f_7+F^i_{nm}f_3f_7+G^i_{nm}f_8f_7).$$

For $0<v\leq i-1$,

$$A^{i+1}_{v,0}=\sum_{m=0}^{i-2}\left[f_2\left(\frac{1}{v}A^i_{v-1,m}+\sum_{n=v}^{i-2}A^i_{nm}f_9\right)+f_5\left(\frac{1}{v}C^i_{v-1,m}+\sum_{n=v}^{i-3}C^i_{nm}f_9\right)+f_7\left(\frac{1}{v}E^i_{v-1,m}+\sum_{n=v}^{i-2}E^i_{nm}f_9\right)\right].$$

For $0<w\leq i-1$,

$$A^{i+1}_{0,w}=\sum_{n=0}^{i-2}\left[f_1\left(\frac{1}{w}A^i_{n,w-1}+\sum_{m=w}^{i-2}A^i_{nm}f_{10}\right)+f_3\left(\frac{1}{w}B^i_{n,w-1}+\sum_{m=w}^{i-2}B^i_{nm}f_{10}\right)\right].$$

For $0<v\leq i-1$ and $0<w\leq i-1$,

$$A^{i+1}_{vw}=\sum_{n=v}^{i-2}\sum_{m=w}^{i-2}A^i_{nm}f_9f_{10}+\frac{1}{v}\sum_{m=w}^{i-2}A^i_{v-1,m}f_{10}+\frac{1}{w}\sum_{n=v}^{i-2}A^i_{n,w-1}f_9+\frac{1}{vw}A^i_{v-1,w-1},$$

$$B^{i+1}_{0,0}=\sum_{n=0}^{i-2}\sum_{m=0}^{i-2}(-A^i_{nm}f_8f_2+B^i_{nm}f_4f_2-C^i_{nm}f_8f_5+D^i_{nm}f_4f_5-E^i_{nm}f_8f_7+F^i_{nm}f_4f_7+G^i_{nm}f_8f_7).$$

For $0<v\leq i-2$,

$$B^{i+1}_{v,0}=\sum_{m=0}^{i-2}\left[f_2\left(-\frac{1}{v}B^i_{v-1,m}+\sum_{n=v}^{i-3}B^i_{nm}f_9(-1)^{n-v}\right)+f_5\left(-\frac{1}{v}D^i_{v-1,m}+\sum_{n=v}^{i-3}D^i_{nm}f_9(-1)^{n-v}\right)+f_7\left(-\frac{1}{v}F^i_{v-1,m}+\sum_{n=v}^{i-3}F^i_{nm}f_9(-1)^{n-v}\right)\right].$$

For $0<w\leq i-1$,

$$B^{i+1}_{0,w}=\sum_{n=0}^{i-2}\left[-f_8\left(\frac{1}{w}A^i_{n,w-1}+\sum_{m=w}^{i-2}A^i_{nm}f_{10}\right)+f_4\left(\frac{1}{w}B^i_{n,w-1}+\sum_{m=w}^{i-2}B^i_{nm}f_{10}\right)\right].$$

For $0<v\leq i-2$ and $0<w\leq i-1$,

$$B^{i+1}_{vw}=\sum_{n=v}^{i-3}\sum_{m=w}^{i-2}B^i_{nm}f_9f_{10}(-1)^{n-v}-\frac{1}{v}\sum_{m=w}^{i-2}B^i_{v-1,m}f_{10}+\frac{1}{w}\sum_{n=v}^{i-2}B^i_{n,w-1}f_9(-1)^{n-v}-\frac{1}{vw}B^i_{v-1,w-1},$$

$$C^{i+1}_{0,0}=\sum_{n=0}^{i-2}\sum_{m=0}^{i-2}(-A^i_{nm}f_1f_7-B^i_{nm}f_3f_7+C^i_{nm}f_1f_6+D^i_{nm}f_3f_6+E^i_{nm}f_1f_7+F^i_{nm}f_3f_7+G^i_{nm}f_8f_7).$$

For $0<v\leq i-2$,

$$C_{v,0}=\sum_{m=0}^{i-2}\left[-f_7\left(\frac{1}{v}A^i_{v-1,m}+\sum_{n=v}^{i-2}A^i_{nm}f_9\right)+f_6\left(\frac{1}{v}C^i_{v-1,m}+\sum_{n=v}^{i-3}C^i_{nm}f_9\right)+f_7\left(\frac{1}{v}E^i_{v-1,m}+\sum_{n=v}^{i-2}E^i_{nm}f_9\right)\right].$$

For $0<w\leq i-2$,

$$C_{0,w}^{i+1}=\sum_{n=0}^{i-2}\left[f_1\left(-\frac{1}{w}C_{n,w-1}^{i}+\sum_{m=w}^{i-3}C_{nm}^{i}f_{10}(-1)^{m-w}\right)+f_3\left(-\frac{1}{w}D_{n,w-1}^{i}+\sum_{m=w}^{i-3}D_{nm}^{i}f_{10}(-1)^{m-w}\right)\right].$$

For $0<v\leq i-2$ and $0<w\leq i-2$,

$$C_{vw}^{i+1}=\sum_{n=v}^{i-3}\sum_{m=w}^{i-3}C_{nm}^{i}f_9f_{10}(-1)^{m-w}+\frac{1}{v}\sum_{m=w}^{i-3}C_{v-1,m}^{i}f_{10}(-1)^{m-w}-\frac{1}{w}\sum_{n=v}^{i-3}C_{n,w-1}^{i}f_9-\frac{1}{vw}C_{v-1,w-1}^{i},$$

$$D_{0,0}^{i+1}=\sum_{n=0}^{i-2}\sum_{m=0}^{i-2}(A_{nm}^{i}f_8f_7-B_{nm}^{i}f_4f_7-C_{nm}^{i}f_8f_6+D_{nm}^{i}f_4f_6-E_{nm}^{i}f_8f_7+F_{nm}^{i}f_4f_7+G_{nm}^{i}f_8f_7).$$

For $0<v\leq i-2$,

$$D_{v,0}=\sum_{m=0}^{i-2}\left[-f_7\left(-\frac{1}{v}B_{v-1,m}^{i}+\sum_{n=v}^{i-3}B_{nm}^{i}f_9(-1)^{n-v}\right)+f_6\left(-\frac{1}{v}D_{v-1,m}^{i}+\sum_{n=v}^{i-3}D_{nm}^{i}f_9(-1)^{n-v}\right)+f_7\left(-\frac{1}{v}F_{v-1,m}^{i}+\sum_{n=v}^{i-3}F_{nm}^{i}f_9(-1)^{n-v}\right)\right].$$

For $0<w\leq i-2$,

$$D_{0,w}^{i+1}=\sum_{n=0}^{i-2}\left[-f_8\left(-\frac{1}{w}C_{n,w-1}^{i}+\sum_{m=w}^{i-3}C_{nm}^{i}f_{10}(-1)^{m-w}\right)+f_4\left(-\frac{1}{w}D_{n,w-1}^{i}+\sum_{m=w}^{i-3}D_{nm}^{i}f_{10}(-1)^{m-w}\right)\right].$$

For $0<v\leq i-2$ and $0<w\leq i-2$,

$$D_{vw}^{i+1}=\sum_{n=v}^{i-3}\sum_{m=w}^{i-3}D_{nm}^{i}f_9f_{10}(-1)^{n+m-v-w}-\frac{1}{v}\sum_{m=w}^{i-3}D_{v-1,m}^{i}f_{10}(-1)^{m-w}-\frac{1}{w}\sum_{n=v}^{i-3}D_{n,w-1}^{i}f_9(-1)^{n-v}+\frac{1}{vw}D_{v-1,w-1}^{i},$$

$$E_{0,0}^{i+1}=\sum_{n=0}^{i-2}\sum_{m=0}^{i-2}(A_{nm}^{i}f_1f_{11}+B_{nm}^{i}f_3f_{11}+C_{nm}^{i}f_1f_{12}+D_{nm}^{i}f_3f_{12}+E_{nm}^{i}f_1f_{13}+F_{nm}^{i}f_3f_{13}+G_{nm}^{i}f_8f_{13}).$$

For $0<v\leq i-1$,

$$E_{v,0}=\sum_{m=0}^{i-2}\left[f_{11}\left(\frac{1}{v}A_{v-1,m}^{i}+\sum_{n=v}^{i-2}A_{nm}^{i}f_9\right)+f_{12}\left(\frac{1}{v}C_{v-1,m}^{i}+\sum_{n=v}^{i-3}C_{nm}^{i}f_9\right)+f_{13}\left(\frac{1}{v}E_{v-1,m}^{i}+\sum_{n=v}^{i-2}E_{nm}^{i}f_9\right)\right].$$

For $0<w\leq i-1$,

$$E_{0,w}^{i+1}=\sum_{n=0}^{i-2}\left[f_1\left(\frac{1}{w}E_{n,w-1}^{i}+\sum_{m=w}^{i-2}E_{nm}^{i}f_{10}\right)+f_3\left(\frac{1}{w}F_{n,w-1}^{i}+\sum_{m=w}^{i-3}F_{nm}^{i}f_{10}\right)+f_8\left(\frac{1}{w}G_{n,w-1}^{i}+\sum_{m=w}^{i-2}G_{nm}^{i}f_{10}\right)\right].$$

For $0<v\leq i-1$ and $0<w\leq i-1$,

$$E_{vw}^{i+1}=\sum_{n=v}^{i-2}\sum_{m=w}^{i-2}E_{nm}^{i}f_9f_{10}+\frac{1}{v}\sum_{m=w}^{i-2}E_{v-1,m}^{i}f_{10}+\frac{1}{w}\sum_{n=v}^{i-2}E_{n,w-1}^{i}f_9+\frac{1}{vw}E_{v-1,w-1}^{i},$$

$$F_{0,0}^{i+1}=\sum_{n=0}^{i-2}\sum_{m=0}^{i-2}(-A_{nm}^{i}f_8f_{11}+B_{nm}^{i}f_4f_{11}-C_{nm}^{i}f_8f_{12}+D_{nm}^{i}f_4f_{12}-E_{nm}^{i}f_8f_{13}+F_{nm}^{i}f_4f_{13}+G_{nm}^{i}f_8f_{13}).$$

For $0<v\leq i-2$,

$$F_{v,0}=\sum_{m=0}^{i-2}\left[f_{11}\left(-\frac{1}{v}B_{v-1,m}^{i}+\sum_{n=v}^{i-3}B_{nm}^{i}f_9(-1)^{n-v}\right)+f_{12}\left(-\frac{1}{v}D_{v-1,m}^{i}+\sum_{n=v}^{i-3}D_{nm}^{i}f_9(-1)^{n-v}\right)+f_{13}\left(-\frac{1}{v}F_{v-1,m}^{i}+\sum_{n=v}^{i-3}F_{nm}^{i}f_9(-1)^{n-v}\right)\right].$$

For $0<w\leq i-2$,

$$F_{0,w}^{i+1}=\sum_{n=0}^{i-2}\left[-f_8\left(\frac{1}{w}E_{n,w-1}^{i}+\sum_{m=w}^{i-2}E_{nm}^{i}f_{10}\right)+f_4\left(\frac{1}{w}F_{n,w-1}^{i}+\sum_{m=w}^{i-3}F_{nm}^{i}f_{10}\right)+f_8\left(\frac{1}{w}G_{n,w-1}^{i}+\sum_{m=w}^{i-2}G_{nm}^{i}f_{10}\right)\right].$$

For $0<v\leq i-2$ and $0<w\leq i-2$,

$$F^{i+1}_{vw}=\sum_{n=v}^{i-3}\sum_{m=w}^{i-3}F^i_{nm}f_9f_{10}(-1)^{n-v}-\frac{1}{v}\sum_{m=w}^{i-3}F^i_{v-1,m}f_{10}+\frac{1}{w}\sum_{n=v}^{i-3}F^i_{n,w-1}f_9(-1)^{n-v}-\frac{1}{vw}F^i_{v-1,w-1},$$

$$G^{i+1}_{0,0}=\sum_{n=0}^{i-2}\sum_{m=0}^{i-2}(A^i_{nm}f_{14}f_{11}+B^i_{nm}f_{15}f_{11}+C^i_{nm}f_{14}f_{12}+D^i_{nm}f_{15}f_{12}+E^i_{nm}f_{14}f_{13}+F^i_{nm}f_{15}f_{13}+G^i_{nm}f_{16}f_{13}).$$

For $0<v\leq i-1$,

$$G_{v,0}=\sum_{m=0}^{i-2}\left[f_{13}\left(\frac{1}{v}G^i_{v-1,m}+\sum_{n=v}^{i-2}G^i_{nm}f_9\right)\right].$$

For $0<w\leq i-1$,

$$G^{i+1}_{0,w}=\sum_{n=0}^{i-2}\left[f_{14}\left(\frac{1}{w}E^i_{n,w-1}+\sum_{m=w}^{i-2}E^i_{nm}f_{10}\right)+f_{15}\left(\frac{1}{w}F^i_{n,w-1}+\sum_{m=w}^{i-3}F^i_{nm}f_{10}\right)+f_{16}\left(\frac{1}{w}G^i_{n,w-1}+\sum_{m=w}^{i-2}G^i_{nm}f_{10}\right)\right].$$

For $0<v\leq i-1$ and $0<w\leq i-1$,

$$G^{i+1}_{vw}=\sum_{n=v}^{i-2}\sum_{m=w}^{i-2}G^i_{nm}f_9f_{10}+\frac{1}{v}\sum_{m=w}^{i-2}G^i_{v-1,m}f_{10}+\frac{1}{w}\sum_{n=v}^{i-2}G^i_{n,w-1}f_9+\frac{1}{vw}G^i_{v-1,w-1},$$

where the subexpressions f_q are given by

$$f_1=\frac{n!}{2^n}-f_8,$$

$$f_2=\frac{m!}{2^m}-f_7,$$

$$f_3=\frac{\hat{H}^{n+1}}{n+1}-\frac{(-1)^n n!}{2^{n+1}},$$

$$f_4=\frac{\hat{H}^{n+1}}{n+1}+\frac{(-1)^n n!}{2^{n+1}},$$

$$f_5=\frac{\hat{L}^{m+1}}{m+1}-\frac{(-1)^m m!}{2^{m+1}},$$

$$f_6=\frac{\hat{L}^{m+1}}{m+1}+\frac{(-1)^m m!}{2^{m+1}},$$

$$f_7=\exp(-2\hat{L})\sum_{p=0}^{m}\frac{\hat{L}^{m-p}m!}{2^{p+1}(m-p)!},$$

$$f_8=\exp(-2\hat{H})\sum_{p=0}^{n}\frac{\hat{H}^{n-p}n!}{2^{p+1}(n-p)!},$$

$$f_9=\frac{n!}{2^{n-v+1}v!},$$

$$f_{10}=\frac{m!}{2^{m-w+1}w!},$$

$$f_{11}=\frac{\hat{L}^{m+1}}{m+1}+\frac{m!}{2^{m+1}}-f_7,$$

$$f_{12}=\frac{\hat{L}^{m+1}}{m+1}+\exp(2\hat{L})\sum_{p=0}^{m}\frac{\hat{L}^{m-p}(-1)^p m!}{2^{p+1}(m-p)!}-\frac{m!(-1)^m}{2^{m+1}},$$

$$f_{13}=f_7+\frac{m!}{2^{m+1}}-\frac{\hat{L}^{m+1}}{m+1},$$

$$f_{14}=\frac{\hat{H}^{n+1}}{n+1}+\frac{n!}{2^{n+1}}-f_8,$$

$$f_{15}=\frac{\hat{H}^{n+1}}{n+1}+\exp(2\hat{H})\sum_{p=0}^{n}\frac{\hat{H}^{n-p}(-1)^p n!}{2^{p+1}(n-p)!}-\frac{n!(-1)^n}{2^{n+1}},$$

$$f_{16}=f_8+\frac{n!}{2^{n+1}}-\frac{\hat{H}^{n+1}}{n+1}.$$

The recurrences for the coefficients begin with $i=3$, for which the coefficients are

$$A^3_{0,0}=1-\frac{1}{2}e^{-2\hat{H}}+\frac{1}{4}e^{-2\hat{L}-2\hat{H}},$$

$$A^3_{1,0}=A^3_{1,1}=1,$$

$$A^3_{0,1}=1-\frac{1}{2}e^{-2\hat{H}},$$

$$B^3_{0,0}=-\frac{1}{2}e^{-2\hat{H}}+\frac{1}{4}e^{-2\hat{L}-2\hat{H}},$$

$$B^3_{0,1}=-\frac{1}{2}e^{-2\hat{H}},$$

$$C^3_{0,0}=D^3_{0,0}=\frac{1}{4}e^{-2\hat{L}-2\hat{H}},$$

$$E^3_{0,0}=1-\frac{1}{4}e^{-2\hat{H}}-\frac{\hat{L}}{2}e^{-2\hat{H}}+\frac{1}{4}e^{-2\hat{L}-2\hat{H}},$$

$$E^3_{1,0}=E^3_{0,1}=E^3_{1,1}=1,$$

$$F^3_{0,0}=-\frac{1}{4}e^{-2\hat{H}}-\frac{\hat{L}}{2}e^{-2\hat{H}}+\frac{1}{4}e^{-2\hat{L}-2\hat{H}},$$

$$G^3_{0,0}=\left(\frac{1}{2}+\hat{H}-\frac{1}{2}e^{-2\hat{H}}\right)\left(\frac{1}{2}+\hat{L}-\frac{1}{2}e^{-2\hat{L}}\right)+\frac{1}{2}-\hat{L}+\frac{1}{2}e^{-2\hat{L}},$$

$$G^3_{1,0}=\frac{1}{2}-\hat{L}+\frac{1}{2}e^{-2\hat{L}},$$

$$G^3_{0,1}=G^3_{1,1}=1.$$

The partition function in Eq. (6) can now be written as

$$Z=(\beta k)^{-2N}\sum_{n=0}^{N-2}\sum_{m=0}^{N-2}(A^N_{nm}f_{19}f_{20}+B^N_{nm}f_{21}f_{20}+C^N_{nm}f_{19}f_{22}+D^N_{nm}f_{21}f_{22}+E^N_{nm}f_{19}f_{18}+F^N_{nm}f_{21}f_{18}+G^N_{nm}f_{17}f_{18}), \tag{A1}$$

where

$$f_{17}=2\exp(-\hat{H})\sum_{p=0}^{n}\frac{\hat{H}^{n-p}n!}{(n-p)!},$$

$$f_{18}=2\exp(-\hat{L})\sum_{p=0}^{m}\frac{\hat{L}^{m-p}m!}{(m-p)!},$$

$$f_{19}=2n!-f_{17},$$

$$f_{20}=2m!-f_{18},$$

$$f_{21}=2\exp(\hat{H})\sum_{p=0}^{n}\frac{\hat{H}^{n-p}(-1)^p n!}{(n-p)!}-2n!(-1)^n,$$

$$f_{22}=2\exp(\hat{L})\sum_{p=0}^{m}\frac{\hat{L}^{m-p}(-1)^p m!}{(m-p)!}-2m!(-1)^m.$$

In order to obtain $dZ/d\hat{H}$, which is needed for calculating the force, one can differentiate Eq. (A1) with respect to $\hat{H}$. The resulting equation contains derivatives of the coefficients with respect to $\hat{H}$, e.g., $dA^N_{nm}/d\hat{H}$, etc. By differentiating the various recurrence relations given above, one obtains recurrence relations for these derivatives. These recurrences again begin with $i=3$, the values of the derivatives there being calculated by taking the derivatives with respect to $\hat{H}$ of the values of the coefficients at $i=3$. This procedure is straightforward, although tedious, and to conserve space the resulting equations are not given here.

The coefficients for $i=N$ contain the information about the density distribution of the end monomers of the chain, which can be obtained without any further calculation. In order to compute the density distribution of every other monomer in the chain, and hence the total monomer density, it would be necessary to derive another set of coefficients obeying somewhat more complicated recurrences, obtained by evaluating the partition function by beginning with the integrals for $i=N$. The need for additional coefficients arises because the chain is fixed at one end and not at the other. Although the calculation is in principle straightforward, the amount of effort required is more than that already expended in obtaining Z, and so is not attempted here.

In order to evaluate the above expressions to obtain Z and $dZ/d\hat{H}$, it is useful to rescale the coefficients in order to prevent their magnitudes from varying too wildly. The following scaling is fairly natural, and leads to some simplifications in the form of the expressions

$$\overline{A^i_{n,m}}=A^i_{n,m}\frac{n!m!}{2^{2i-n-m}},$$

where the coefficient on the left-hand side with the bar represents the scaled version, and similarly for the other coefficients.

[1] D.E. Smith, H.P. Babcock, and S. Chu, Science **283**, 1724 (1999).

[2] M.S.Z. Kellermayer, S.B. Smith, C. Bustamante, and H.L. Granzier, J. Struct. Biol. **122**, 197 (1998).

[3] B.J. Haupt, J. Ennis, and E.M. Sevick, Langmuir **15**, 3886 (1999).

[4] P.-G. de Gennes, *Scaling Concepts in Polymer Physics* (Cornell University Press, Ithaca, 1979).

[5] M. Doi and S.F. Edwards, *The Theory of Polymer Dynamics* (Clarendon Press, New York, 1986).

[6] M.C. Guffond, D.R.M. Williams, and E.M. Sevick, Langmuir **21**, 5691 (1997).

[7] G. Subramanian, D.R.M. Williams, and P.A. Pincus, Europhys. Lett. **29**, 285 (1995).

[8] G. Subramanian, D.R.M. Williams, and P.A. Pincus, Macromolecules **29**, 4045 (1996).

[9] D.R.M. Williams and F.C. MacKintosh, J. Phys. II **9**, 1417 (1995).

[10] J. Jimenez and R. Rajagopalan, Langmuir **14**, 2598 (1998).

[11] J. Jimenez and R. Rajagopalan, Eur. Phys. J. B **5**, 237 (1998).

[12] G.A. Arteca, Int. J. Quantum Chem. **65**, 219 (1997).

[13] A. Milchev, V. Yamakov, and K. Binder, Phys. Chem. Chem. Phys. **1** 2083 (1999).

[14] A. Milchev, V. Yamakov, and K. Binder, Europhys. lett. **47**, 675 (1999).

[15] E.M. Sevick and D.R.M. Williams, Macromolecules (to be published).

[16] J. Ennis and B. Jönsson, J. Phys. Chem. **103**, 2248 (1999).

[17] FORTRAN90 code is available from Jonathan Ennis, who can be contacted at j.ennis-king@dpr.csiro.au